AD-A042 368 ROCKWELL INTERNATIONAL ANAHEIM CALIF ELECTRONICS RES--ETC F/G 9/2
HIGH DENSITY MAGNETIC BUBBLE MEMORY TECHNIQUES.(U)
JUN 77 P J BESSER, D M HEINZ, T KOBAYASHI F33615-76-C-1198

UNCLASSIFIED C76-845.7/501 AFAL-TR-77-17 NL

| OF |
ADA
042368

END

DATE
FILMED
8-77

AFAL-TR-77-17

12

HIGH DENSITY MAGNETIC BUBBLE MEMORY TECHNIQUES

ELECTRONICS RESEARCH CENTER
ROCKWELL INTERNATIONAL
ANAHEIM, CALIFORNIA

JUNE 1977

TECHNICAL REPORT AFAL–TR–77–17
INTERIM REPORT FOR 4 MAY 1976 TO 4 NOVEMBER 1976

Approved for public release; distribution unlimited

AIR FORCE AVIONICS LABORATORY
AIR FORCE WRIGHT AERONAUTICAL LABORATORIES
AIR FORCE SYSTEMS COMMAND
WRIGHT–PATTERSON AFB, OHIO 45433

AFAL-TR-77-17

NOTICE

When Government drawings, specifications, or other data are used for any purpose other than in connection with a definitely related Government procurement operation, the United States Government thereby incurs no responsibility nor any obligation whatsoever; and the fact that the government may have formulated, furnished, or in any way supplied the said drawings, specifications, or other data, is not to be regarded by implication or otherwise as in any manner licensing the holder or any other person or corporation, or conveying any rights or permission to manufacture, use, or sell any patented invention that may in any way be related thereto.

This report has been reviewed by the Information Office (OI) and is releasable to the National Technical Information Service (NTIS). At NTIS it will be available to the general public, including foreign nations.

This technical report has been reviewed and is approved for publication.

Millard G. Mier

MILLARD G. MIER
Project Engineer

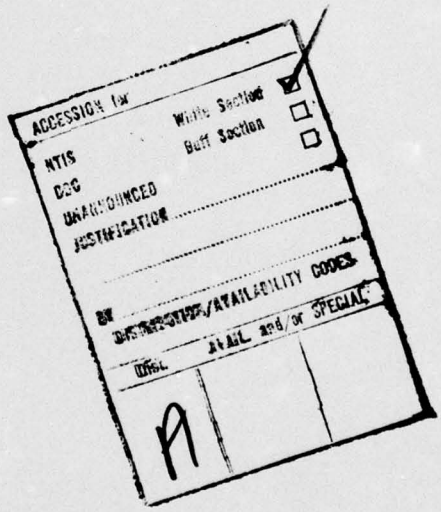

FOR THE COMMANDER

Robert D. Larson

ROBERT D. LARSON, Chief
Electronic Research Branch
Electronic Technology Div.
AF Avionics Laboratroy

Copies of this report should not be returned unless return is required by security considerations, contractural obligations, or notice on a specific document.

UNCLASSIFIED

SECURITY CLASSIFICATION OF THIS PAGE (When Data Entered)

REPORT DOCUMENTATION PAGE	READ INSTRUCTIONS BEFORE COMPLETING FORM
1. REPORT NUMBER: AFAL-TR-77-17	2. GOVT ACCESSION NO. / 3. RECIPIENT'S CATALOG NUMBER
4. TITLE (and Subtitle): HIGH DENSITY MAGNETIC BUBBLE MEMORY TECHNIQUES.	5. TYPE OF REPORT & PERIOD COVERED: 4 May 1976 to 4 Nov 1976 Interim
	6. PERFORMING ORG. REPORT NUMBER: C76-845.7/501
7. AUTHOR(s): P. J. Besser, T. Kobayashi, D. M. Heinz, T. Chen	8. CONTRACT OR GRANT NUMBER(s): F33615-76-C-1198
9. PERFORMING ORGANIZATION NAME AND ADDRESS: Rockwell International, Electronics Research Division, Anaheim, California	10. PROGRAM ELEMENT, PROJECT, TASK AREA & WORK UNIT NUMBERS: 61102F, 2305/R2/61
11. CONTROLLING OFFICE NAME AND ADDRESS: Air Force Avionics Laboratory, (DHR), Wright-Patterson AFB, Ohio 45433	12. REPORT DATE: June 1977
	13. NUMBER OF PAGES: 41
14. MONITORING AGENCY NAME & ADDRESS (if different from Controlling Office): Interim rept. 4 May – 4 Nov 76, 33p.	15. SECURITY CLASS. (of this report): Unclassified
	15a. DECLASSIFICATION/DOWNGRADING SCHEDULE

16. DISTRIBUTION STATEMENT (of this Report)

Approved for public release; distribution unlimited.

17. DISTRIBUTION STATEMENT (of the abstract entered in Block 20, if different from Report)

18. SUPPLEMENTARY NOTES

19. KEY WORDS (Continue on reverse side if necessary and identify by block number)

Small Bubble Materials
Self Biased Materials/Devices
High Capacity Chip Design

20. ABSTRACT (Continue on reverse side if necessary and identify by block number)

Several material compositions have been investigated with the goal of obtaining a material suitable for operation in devices requiring bubble domain diameters of ≤1μm. An YSmTmGaIG composition has shown attractive material properties and has been submitted for device evaluation.

Analysis of self-biased structures has been performed. The results show a dependence of the effective bias field on the quality factor q. This analysis has provided improved

DD FORM 1 JAN 73 1473 EDITION OF 1 NOV 65 IS OBSOLETE

UNCLASSIFIED

SECURITY CLASSIFICATION OF THIS PAGE (When Data Entered)

407 912

criteria for selection of the optimum parameters for temperature stable self-biased materials/devices.

Component designs for a hybrid decoder chip and a wafer level integration approach to a high capacity chip have been completed. A test chip incorporating several versions of the components has been submitted for fabrication and evaluation.

A conceptual study of a 10^{12} bit data storage system has been initiated.

10 to the 12th power

FOREWORD

This is an Interim Report on Contract F33615-76-C-1198 covering the period 4 May 1976 to 4 November 1976. The research effort was performed in the Applied Magnetics and Solid State Materials Research Branches of the Physical Sciences Department. Dr. P. J. Besser is the Program Manager and Principal Investigator. Other major contributors to the program for this interval and their areas of effort are: Dr. D. M. Heinz, Materials Research, Dr. T. Kobayashi, Material/Device Interface studies, and Dr. T. T. Chen, High Capacity Device Development.

TABLE OF CONTENTS

LIST OF ILLUSTRATIONS

LIST OF TABLES

SECTION I

INTRODUCTION

The objective of this basic research effort is to demonstrate the feasibility of a new technology for all solid state large data base memories for airborne/spaceborne applications. The program scope is limited to demonstrating the feasibility of the device functions and bit density capabilities required to meet the system goals of Table 1.

TABLE 1
Large Data Base Memory System Goals

Parameter	Minimum Goals
Capacity	10^{12} bits
Block Size	10^{7} bits
Access Time to a Block	10^{-4} sec read/write
Reliability (Untended MTBF)	10^{5} Hr
Volatility (Standby Retention Time)	1 year
Volume	2 Cubic ft
Weight	120 lb
Power	200 W
In/Out Data Rate	5×10^{7} Bits/Sec
Ambient Temperature Range (Operating)	-55°C to $+125^{\circ}$C

It is the goal of this program to advance one technology into development. Based on an evaluation of the present and potential capabilities of candidate solid state technologies to meet the Table 1 targets, magnetic bubble domain technology has been selected as the one to be pursued on this program.

The proposed approach makes use of small bubble materials, self-biased materials and devices, wafer level integration using hybrid chip designs and fineline lithographic techniques for device fabrication. In this report interval, emphasis has been on small bubble materials research and development (Section 2), analysis of self-biased structures (Section 3), self biased material/device interface studies (Section 4) and high capacity device design (Section 5). A conceptual study of a 10^{12} bit system is in the early stages (Section 6).

SECTION II

SMALL BUBBLE MATERIALS

The first material development task on this program is the preparation of an improved 1 μm bubble composition. In order to establish a valid basis for the evaluation of this new material, it was decided to grow films with a target stripwidth of 2 μm first, so that a direct comparison could be made with previously developed 2 μm bubble materials. Once an improved 2 μm bubble composition was developed, the melt composition would be adjusted to grow 1 μm bubble material. During the past half-year, three compositions have been evaluated for 2 μm bubbles and one composition has been evaluated for 1 μm bubbles.

The major material parameter requirement for the formation of bubble domains is that the quality factor q be greater than unity, where q is defined as

$$q = K_u / 2\pi M_s^2 ,$$

K_u is the uniaxial anisotropy and $4\pi M_s$ is the saturation magnetization. A low value of q (of about 2) permits spontaneous bubble nucleation to occur (causing the loss of stored information) in high gradient field regions, as beneath the permalloy pattern elements in a field-accessed device or beneath a drive conductor in a current-accessed device. With increasing temperature, M_s^2 decreases more slowly than K_u so that q decreases. For stable device operation at 50°C, device studies have shown that a room temperature q of about 4 is required.

In a garnet film with a thickness which is approximately equal to its bubble diameter, the saturation magnetization increases with decreasing bubble size. Four μm bubble materials have $4\pi M_s$ values of 200 to 300 G, 2 μm bubble materials have $4\pi M_s$ values of 400 to 550 G and 1μm bubble materials have $4\pi M_s$ values of 600 to 800 G. In order to retain q values of 4 as we decrease the bubble diameter, we see from the definition of q that the value of K_u must increase rapidly. Thus, for 4μm bubbles K_u must be 6 to 14 K Erg/cm^3, for 2μm bubbles K_u must be 25 to 48 K Erg/cm^3, and for 1μm bubbles K_u must be 60 to 100 K Erg/cm^3. This calls for increasing K_u by a factor of 3 to 4 on going from currently used 4μm bubble material to 2μm bubble material and increasing K_u by a factor of 7 to 10 on going from 4μm bubble material to 1μm bubble material.

K_u may be introduced in epitaxial garnet films as a consequence of: (1) the inverse magnetostriction effect caused by stress between film and substrate due to lattice parameter mismatch, K^S_u, and (2) chemical constituents and growth conditions, K^G_u. Since K^G_u may exceed K^S_u by a factor of 10 or more, it is of primary concern for increasing q. In a practical way, at present we are limited to a few guidelines for controlling K_u in films that we grow. First, garnet films grown by liquid phase epitaxy at lower temperatures have higher K^G_u due to the incorporation of Pb from the flux, and hence must be grown with due regard to film/substrate lattice parameter mismatch considerations. (Pb is a large ion which expands the garnet lattice parameter to the extent that it is incorporated into a film.) Second, Sm and Eu contribute to high K^G_u while the spherical ions Y, La, Gd, Lu and Ca act as diluents. Third, in a mixed rare earth composition, the greater the difference in rare earth size, the greater the K^G_u. And fourth, K^S_u should be as large as practical and should be in a sense that is additive to K^G_u.

The small bubble compositions we have worked with in the past have been in the systems $(YSm)_3(FeGa)_5O_{12}$ and $(YEuTm)_3(FeGa)_5O_{12}$. Two μm bubble compositions in these systems have K_u values in the range of 20 to 30 K Erg/cm^3, q values in the range of 3 to 4 and Neel temperature values, T_N, in the range of 135 to 155°C. Since we wanted a material with a higher K_u and a higher T_N, the first composition chosen was $Y_{1.8}Sm_{0.2}Er_{0.2}Ca_{0.8}Fe_{4.2}Ge_{0.8}O_{12}$. The combination of Sm and Er was expected to provide a high K^G_u as in the early bubble composition $(EuEr)_3(FeGa)_5O_{12}$, and Ca-Ge substitution was expected to yield a higher T_N than Ga substitution.

A melt of this composition was formulated and a number of films were grown. During the growth of a series of films, the concentrations of Ca and Ge were changed to investigate their influence on K_u. All of the films grown from this melt had T_N values in the range of 205 to 215°C, an increase of 60 to 70°C over previous values. In most of these films with high Ca content, normal bubble generation techniques for material characterization produced hard bubbles and valid collapse fields could not be obtained. After ion implantation to provide hard bubble suppression, the static properties were measured. The K_u values were found to lie in the range of 7 to 33 K Ergs/cm^3 with q values of 2.1 to 3.6, except one which had a q value of 4.5. The K_u and q values were lower than anticipated, being comparable to previously grown films. We found that all of the films were in compressive stress which caused K^S_u to subtract from K^G_u. This compressive stress may have been due to the presence of Er on octahedral sites. In addition, these films exhibited high coercivities. Thus, it was concluded that this melt formulation was not adequate for small bubble material.

In the interest of preparing 2 μm bubble films with larger values of q, a second melt formulation was investigated. Due to the problem of high coercivity in the Ca-Ge melt, it was decided to develop a Ga-substituted composition with suitable properties first, and prepare a Ca-Ge composition later to obtain the higher T_N. The composition selected was $Y_{2.0}Sm_{0.5}Er_{0.5}Fe_4Ge_1O_{12}$. This formulation has a greater concentration of rare earth ions than previously studied compositions, which should increase K^G_u and q but decrease μ_w, the wall mobility. For preliminary small bubble device work, however, a high q is more important than a high μ_w.

A melt of this composition was formulated and films were grown. The higher rare earth concentrations in these films yielded slightly higher q values of 3.1 to 5.1, although the film with the highest q was too thick (2.40 μm). Due to the disappointingly low values of K_u from the Sm-Er films, work with this system was terminated.

In light of the large K^G_u values obtained in the past from the $(YEuTm)_3(FeGa)_5O_{12}$ and $(YGdTm)_3(FeGa)_5O_{12}$ systems, the third melt composition to be investigated on this program was $Y_{2.0}Sm_{0.5}Tm_{0.5}Fe_{4.1}Ga_{0.9}O_{12}$. Here we have substituted the smaller rare earth Tm in place of Er of the previous melt composition with the expectation of a larger value of q. For a stripwidth of 1.7 μm and a thickness of 1.7 μm, this composition yielded K_u values of 25 to 60 K Erg/cm^3, q values of 3.4 to 5.6, and $4\pi M_s$ values of 435 to 536 G.

Since these K_u values were the highest we have realized in 2μm bubble materials, the melt was modified to provide 1μm bubble materials. For a stripwidth of 1.0μm and a thickness of 0.8μm, this composition yielded K_u values of 25 to 54 K Erg/cm^3, q values of 1.7 to 2.8, and $4\pi M_s$ values of 600 to 694 G.

The primary objective in the materials investigation was to produce films with the desired properties as quickly as possible. In order to adjust the stripwidth to meet device tolerances, it was usually necessary to make several additions to the melt after its initial formulation. As a result, films were often grown at a rapid rate from a melt with a low or a high R_1 (iron to rare earth ratio), so that the ultimate properties for the nominal composition were not attained. Improved film properties should result from reformulated melt compositions which have preferred values of R_1 and normal growth rates.

In characterizing small bubble materials, measurement of the collapse field becomes very difficult because (1) contrast is poor and the image is fuzzy so that it is hard to see when a bubble collapses, and (2) the strip splitter on our characterization station is unable to cut the domains of materials with high $4\pi M_s$ and high K_u. It has, therefore, been necessary to employ a characterization technique which is much more subjective than measuring the collapse field: The bias field is increased slowly until smooth contraction of the stripes ceases. (Repeating this procedure several times gives some confidence to the technique but it has considerable uncertainty.) This value of the bias field, H_{bias}, is used in conjunction with the ratio of the period at zero bias, P_o, to the film thickness, h, to obtain $4\pi M_s$ from a plot of $H_{bias}/4\pi M_s$ vs P_o/h (Ref 1). Following ion implantation, a few bubbles were often found which were used to make collapse field measurements; however, this type of bubble (generated during ion implantation) is not always typical of bubbles formed in a more conventional way. When a spatial filtering station (Ref 2) for small bubbles has been assembled, we will be in a better position to provide reliable characterization data on small bubble materials.

SECTION III

ANALYSIS OF SELF-BIASED STRUCTURES

One accomplishment which would aid the success of this program is the development of self-biased devices which operate reliably over an extended temperature range. To this end, temperature-stable self-biased films must be grown first. However, the specifications described in previous articles for growing such films seem to be somewhat crude, since many of the films grown thereby tend to be underbiased. It is thus felt that for successful growth of temperature-stable self-biased films for small bubbles a better understanding of the basic physics of self-biasing is necessary. Accordingly, we have carried out an extensive analysis of self-biased structures which will be discussed in this Section.

3.1 INTRODUCTION

Liu, et al (Ref 3) first proposed the idea of internally supplying an effective bias field to stabilize magnetic bubbles via capping domain walls formed at the interface of a bubble film and an additional layer which is exchange-coupled to the bubble film and permanently magnetized opposite to the bubble magnetization. They demonstrated partial replacement of the bias field using an orthoferrite-metal double-layer structure. Double-layer epitaxial garnet films having capping walls were grown by Bobeck, et at (Ref 4) in conjunction with their work on hard bubble suppression. Later, Uchishiba, et al (Refs 5 to 7) grew double-layer epitaxial garnet films with their material parameters adjusted to full self-biasing and demonstrated operation of bubble devices without an external bias field.

Let us briefly review the basic theory of the self-biased structure to understand its basic mechanism. Consider a double layer film as shown in Figure 1. If the bottom layer (layer 1) has an extremely high anisotropy field, H_{K1} ($>> 4\pi M_S$ of either layer), then, once saturated in one direction, it will remain saturated until a field higher than H_{K1} is applied in the opposite direction*.

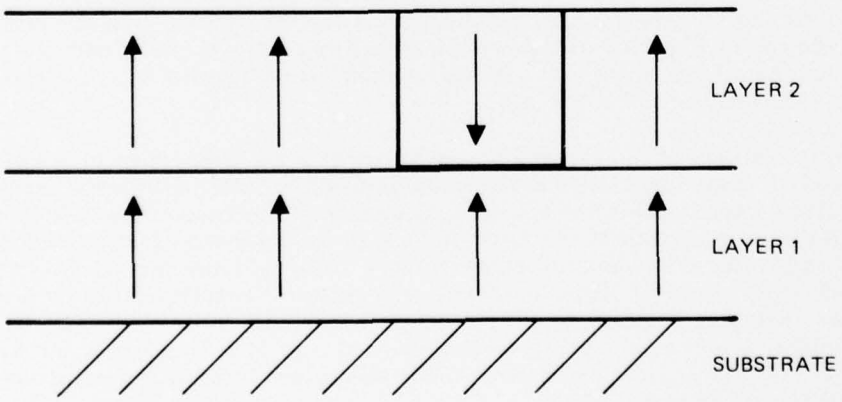

Figure 1. Double Layer Self-Biased Bubble Domain Structure

*A nucleation field is in general much smaller than H_{K1} at the edge of an as-grown wafer or of a sample mechanically cut from a wafer. However, it can be made as large as H_{K1} by chemically etching off the edges (see Section IV).

SECTION III

ANALYSIS OF SELF-BIASED STRUCTURES

One accomplishment which would aid the success of this program is the development of self-biased devices which operate reliably over an extended temperature range. To this end, temperature-stable self-biased films must be grown first. However, the specifications described in previous articles for growing such films seem to be somewhat crude, since many of the films grown thereby tend to be underbiased. It is thus felt that for successful growth of temperature-stable self-biased films for small bubbles a better understanding of the basic physics of self-biasing is necessary. Accordingly, we have carried out an extensive analysis of self-biased structures which will be discussed in this Section.

3.1 INTRODUCTION

Liu, et al (Ref 3) first proposed the idea of internally supplying an effective bias field to stabilize magnetic bubbles via capping domain walls formed at the interface of a bubble film and an additional layer which is exchange-coupled to the bubble film and permanently magnetized opposite to the bubble magnetization. They demonstrated partial replacement of the bias field using an orthoferrite-metal double-layer structure. Double-layer epitaxial garnet films having capping walls were grown by Bobeck, et at (Ref 4) in conjunction with their work on hard bubble suppression. Later, Uchishiba, et al (Refs 5 to 7) grew double-layer epitaxial garnet films with their material parameters adjusted to full self-biasing and demonstrated operation of bubble devices without an external bias field.

Let us briefly review the basic theory of the self-biased structure to understand its basic mechanism. Consider a double layer film as shown in Figure 1. If the bottom layer (layer 1) has an extremely high anisotropy field, H_{K1} ($>> 4\pi M_S$ of either layer), then, once saturated in one direction, it will remain saturated until a field higher than H_{K1} is applied in the opposite direction*.

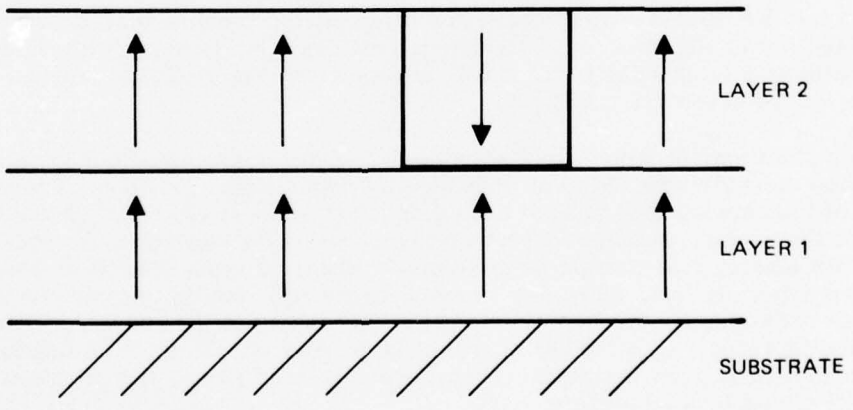

Figure 1. Double Layer Self-Biased Bubble Domain Structure

*A nucleation field is in general much smaller than H_{K1} at the edge of an as-grown wafer or of a sample mechanically cut from a wafer. However, it can be made as large as H_{K1} by chemically etching off the edges (see Section IV).

Under these conditions, a bubble domain in the top layer (layer 2) will be capped with a domain wall at the interface of the two layers. Then, a bubble domain with diameter, d, in layer 2 of thickness, h_2, and saturation magnetization, M_{s2}, has the energy of the form

$$E_T = \frac{1}{2} M_{s2} H_B \pi d^2 h_2 + \pi d h_2 \sigma_{w2} - E_M + \frac{1}{4} \pi d^2 \sigma_{w12} \quad (1)$$

where H_B, σ_{w2}, and σ_{w12} are the external bias field, the wall energy density of layer 2, and the energy density of the capping wall, and E_M is the magnetostatic energy of the bubble. Note the same dependence on d of the first term (Zeeman energy) and the last term (capping wall energy). Taking the partial derivative of E_T with respect to d yields the force stability condition

$$\frac{\ell_2}{h_2} + \frac{d}{h_2}\left(\frac{H_B}{4\pi M_{s2}} + \frac{\ell_{12}}{2h_2}\right) - F\left(\frac{d}{h_2}\right) = 0 \quad (2)$$

where $F(d/h_2)$ is the Thiele force function, (Ref 8) $\ell_2 = \sigma_{w2}/4\pi M_{s2}{}^2$ and $\ell_{12} = \sigma_{w12}/4\pi M_{s2}{}^2$ It is seen from Eq (2) that the capping wall energy provides a normalized effective bias field of magnitude $\ell_{12}/2h_2$. In order for this structure to support stable half bubbles, the wall energy density of layer 1, σ_{w1}, must be higher than that of layer 2, σ_{w2}, since otherwise the capping wall will penetrate into layer 1 and eventually punch through from the layer 1/layer 2 interface to the substrate. Under the condition $\sigma_{w1} > \sigma_{w2}$, the capping wall forms inside layer 2 and its energy density is assumed equal to that of layer 2, (Ref 5, 6, 7, and 9) i.e., $\sigma_{w12} = \sigma_{w2}$. Thus, dropping the suffices, the normalized effective bias field, $H_{eff}/4\pi M_s$ may be written as $\ell/2h$. It should be noted that if an additional biasing layer is placed on top of the bubble supporting layer of Figure 1, the biasing power is exactly doubled. Thus, the effective bias field can be writtin in more general form as

$$\frac{H_{eff}}{4\pi M_s} = \frac{b\ell}{2h} \quad (3)$$

where b = 1 for the "single-biased" case and b = 2 for the "double-biased" case. This relation is plotted in Figure 2 for the single biased case (b = 1) along with the bubble stability range as a function of h/ℓ. It can be seen from Figure 2 that full self-biasing can only be achieved for $2.5 \leq h/\ell \leq 3$.

The implications of the above discussion are that the properties of the self-biased bubble depend strongly upon those of the capping domain wall. Curiously enough, however, the nature of the capping wall has not been discussed in the literature. Obviously, the structure of the capping wall is of "head-on" type. As a consequence, its energy, therefore, its biasing effect might be appreciably different from that of the 180 deg wall of Block type. In fact, there are some experimental results that may be attributed to this. For example, double layer films grown according to the above specifications (i.e., assuming $\sigma_{w12} = \sigma_{w2}$) tend to be underbiased (Ref 5). Thus, it is felt that in order to successfully grow temperature-stable self-biased films, the nature of the capping wall should be studied first.

In the following section, we will look into the structure of the capping wall and derive its wall energy. On the basis of this analysis, we will then discuss the conditions under which self-biased bubbles can be stabilized.

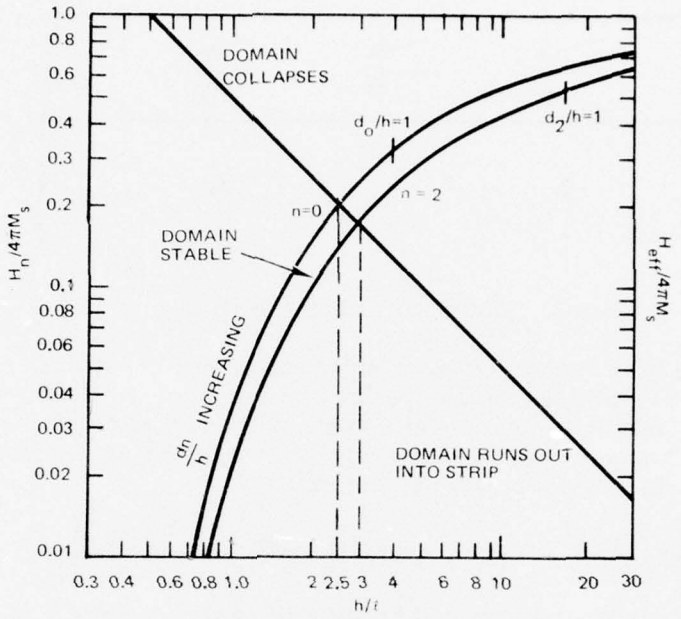

Figure 2. Stability Condition for Self-Biased Bubble Domain

3.2 STRUCTURE AND ENERGY OF THE CAPPING WALL

It is seen from Figure 1 that the capping wall is of the head-on type. Since the bubble is a cylindrical domain, the capping wall must have a radial symmetry. This means that the component of the magnetization vector in the plane of the wall varies its direction. As long as the thickness of the wall is small compared with the radius of the bubble, however, the exchange energy associated with this angular variation is negligible. It is also suggested that the capping wall has some curvature (Ref 4). This is presumably due to a strong radial stray field at the edge of the bubble where the capping wall must be smoothly connected to the vertical wall. The effect of this radial stray field seems to be to increase the thickness of the capping wall. Thus, the wall curvature may be more appropriately termed as radial thickness variation. In any case, however, its effect may be neglected again as long as the radius of the capping wall is much larger than its thickness. Thus, in view of the fact that the capping wall is formed inside layer 2, the capping wall may be approximated by a head-on domain wall in an infinite medium as shown in Figure 3, in which the easy axis is coincident with the z axis ($M_z = \mp M_s$ at $z = \pm\infty$) and the wall lies in the xy plane. As discussed above the variation of the magnetization vector in the xy plane is neglected and its z component, $M_s \cos\theta$, is assumed to depend only on z.

Under the above assumptions the energy per unit area of the wall is the sum of the exchange, anisotropy, and magnetostatic energies and given by

$$\sigma = \int_{-\infty}^{\infty} \left[A\left(\frac{d\theta}{dz}\right)^2 + K_u \sin^2\theta + 2\pi M_s^2 \cos^2\theta \right] dz \qquad (4)$$

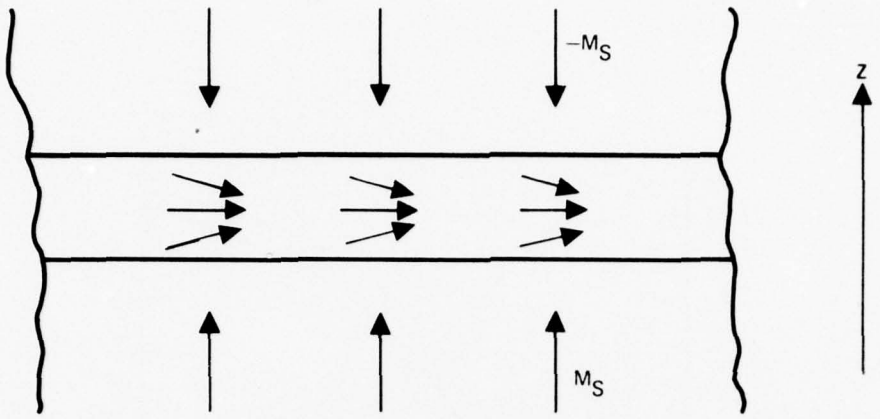

Figure 3. Model for Capping Wall Structure

where A and K_u are the exchange and uniaxial anisotropy constants, respectively. It is noted that the integral does not have a finite value since the magnetostatic energy is $2\pi M_S^2$ at $z = \pm\infty$. However, this infinite value of the magnetostatic energy is not a problem at all. This point can be made apparent by rewriting the last term of Eq (4) as $2\pi M_S^2 (1 - \sin^2\theta)$. Equation (4) then becomes

$$\sigma = \int_{-\infty}^{\infty} \left[A\left(\frac{d\theta}{dz}\right)^2 + \left(K_u - 2\pi M_s^2\right) \sin^2\theta + 2\pi M_s^2 \right] dz \qquad (5)$$

Obviously, it is the last term that makes the wall energy infinite. The last term, which is independent of the magnetization distribution of the wall, is the magnetostatic energy of a uniformly magnetized medium. In our double layer film for which z is terminated at the surface, this magnetostatic energy of course has a finite value and corresponds to the demagnetizing energy of the film. Formation of bubble or strip domains greatly reduces this energy. In other words, going from the infinite medium of Figure 3 to the finite medium and finite domain size of Figure 1, this energy is carried along in the form of the magnetostatic energy of the bubble. Consequently, the capping wall energy can be defined as

$$\sigma_{w12} = \int_{-\infty}^{\infty} \left[A\left(\frac{d\theta}{dz}\right)^2 + \left(K_u - 2\pi M_s^2\right) \sin^2\theta \right] dz \qquad (6)$$

Note that Eq (5) has the same functional form as that of the energy of the simple 180 deg Block wall with K_u replaced by $K_u - 2\pi M_S^2$. Thus, the minimization condition yields

$$\sigma_{w12} = 4 \sqrt{A\,(K_u - 2\pi M_s^2)}$$

$$= \sigma_{w2} \left(1 - \frac{1}{q}\right)^{1/2}$$

where $\sigma_{w2} = 4\sqrt{A\,K_u}$ and $q = K_u / 2\pi M_s^2$

It should be noted that the capping wall energy is smaller than the cylindrical domain wall energy by a factor $(1 - 1/q)^{1/2}$.

Now the effective bias field should be modified to include the above factor. Hence

$$\frac{H_{eff}}{4\pi M_s} = \frac{b\ell}{2h} \left(1 - \frac{1}{q}\right)^{1/2} \tag{7}$$

The implication of this result is twofold. First, the effective bias field is reduced by the factor $(1 - 1/q)^{1/2}$, e.g., 10 percent for $q = 5$. This probably explains the tendency of many films grown under previous specifications (assuming $q \to \infty$) to be underbiased. Secondly, this factor gives rise to an additional temperature dependence. Thus the static stability and temperature dependence of self-biased bubbles must be reconsidered on the basis of this new result.

3.3 STABILITY OF SELF-BIASED BUBBLES

The effective bias field given by Eq (7) is plotted in Figure 4 for the single-biased case ($b = 1$) for $q = \infty$ and $q = 4$. For $q \to \infty$, the effective bias field is unchanged from the simpler expression, Eq (3). For $q < 10$, however, the full biasing condition is considerably different. For $q = 4$, for example, the range of h/ℓ for stability is between 2.25 and 2.7. In practice, both ℓ and q are temperature dependent, making the stability range even narrower. In the following, we discuss stability conditions for self-biased bubbles with temperature.

The stability equation for the self-biased bubble is

$$\frac{\ell}{h} + \frac{d}{h}\left[\frac{b\ell}{2h}\left(1 - \frac{1}{q}\right)^{1/2}\right] - F\left(\frac{d}{h}\right) = 0 \tag{8}$$

If we use Callen and Joseph's approximate expression (Ref 10) for the magnetostatic force term, $F(d/h)$, we can solve Eq (8) for the bubble diameter as a function of ℓ and q, i.e.,

$$\frac{d}{h} = \frac{-\left[\left(\frac{3}{4} + \frac{ab}{2}\right)\frac{\ell}{h} - 1\right] \pm \sqrt{\left[\left(\frac{3}{4} + \frac{ab}{2}\right)\frac{\ell}{h} - 1\right]^2 - \frac{3ab}{2}\left(\frac{\ell}{h}\right)^2}}{\frac{3ab}{4}\left(\frac{\ell}{h}\right)} \tag{9}$$

where $a = (1 - 1/q)^{1/2}$ and b is the number of capping walls per bubble. This relation is plotted in Figure 5 with q as a parameter for $b = 1$ (single-biased) and $b = 2$ (double-biased).

Let us look at the single-biased case first. If q is constant, d varies with ℓ along a solid line with constant q, e.g., line BA for $q = 10$ or line DC for $q = 4$. On the other hand, if ℓ is constant, d varies along a vertical line, e.g., line DF or line AE. If both ℓ and q vary, d will exhibit a complicated locus. For example, if q varies from 10 to 4 and ℓ/h varies from 0.414 to 0.353, d/h will follow locus AD.

In order to obtain a real feeling as to how the bubble diameter varies with ℓ and q, we have tabulated $d_T = \frac{1}{d}\frac{\partial d}{\partial T}$ in Table 2 for various loci assuming the temperature variation is from $0^{\circ}C$ to $50^{\circ}C$ for both the single-biased and the double-biased cases.

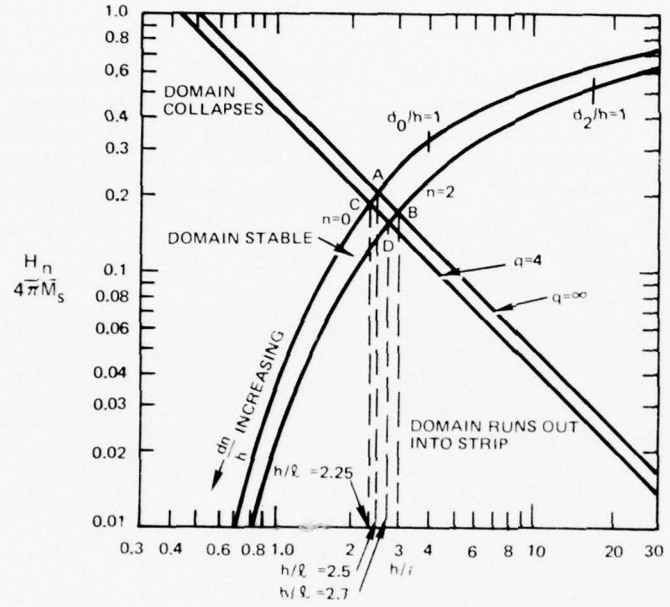

Figure 4. Effect of q Dependence on Self-Biased Bubble Stability Condition

Let us now discuss what the optimum material parameters would be for temperature-stable self-biasing. Consider the single biased case first. For $h/\ell \approx 2.5$, the stable bias field range is $\sim 0.07 \times 4\pi M_S$. Thus, for $4\pi M_S \approx 300$ G, the stable bias field range is about 20 Oe. In a field accessed bubble device, typically the elements of the permalloy overlay provide a negative bias field of 10 Oe. Thus, if the self biasing condition is chosen such that free bubbles are effectively biased in the vicinity of their collapse (along line AC in Figures 2 and 5) the negative field from the permalloy overlay will bring the trapped bubbles into the middle of the stability range. If $4\pi M_S$ is considerably higher than 300 G, i.e., if the stable bias range is considerably wider than 20 Oe, the above condition will produce overbiasing. In other words, a negative bias field from the elements of the permalloy overlay will not be sufficient to bring trapped bubbles into the midpoint of the stability range. In this case, the biasing condition should be chosen such that free bubbles are effectively biased along a line nearly parallel to line AC but somewhat inside the stability range. A similar situation is encountered in the double-biased case where the stable bias range is wider ($\sim 0.1 \times 4\pi M_S$ instead of $\sim 0.07 \times 4\pi M_S$). Nevertheless, choosing the material parameters so as to follow the collapse line is extremely useful for determining the optimum temperature coefficients of ℓ and q, since they are unchanged as long as the material parameters follow a line parallel to line AC. Thus, let us assume that the material parameters are chosen to follow the collapse line AC.

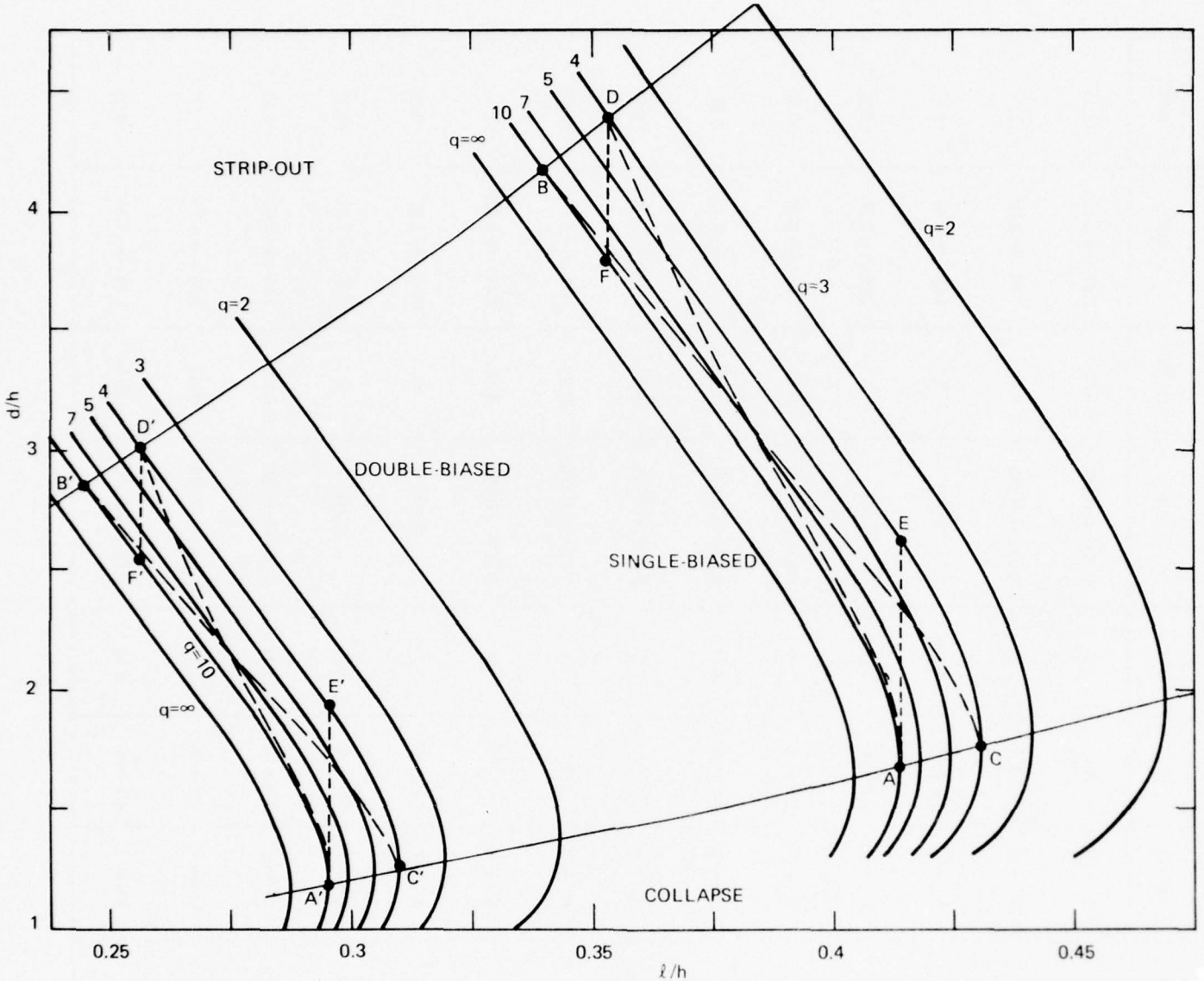

Figure 5. Dependence of Bubble Diameter on ℓ and q for Single and Double Biased Bubbles

TABLE 2

Temperature Variation of Bubble Diameter (Calculated from Eq 9)

b	LOCUS	q	q_T (%/°C)	ℓ/h	ℓ_T (%/°C)	d/h	d_T (%/°C)
1	A → B	10	0	0.414 → 0.340	-0.39	1.68 → 4.17	+1.70
	C → D	4	0	0.431 → 0.353	-0.40	1.76 → 4.38	+1.71
	A → E	10 → 4	-1.71	0.414	0	1.68 → 2.62	+0.87
	F → D	10 → 4	-1.71	0.353	0	3.45 → 3.77	+0.18
	A → D	10 → 4	-1.71	0.414 → 0.353	-0.32	1.68 → 4.38	+1.78
	B → C	10 → 4	-1.71	0.340 → 0.431	+0.47	4.17 → 1.76	-1.63
	A → C	10 → 4	-1.71	0.414 → 0.431	+0.08	1.68 → 1.76	+0.09
2	A′ → B′	10	0	0.295 → 0.245	-0.37	1.19 → 2.85	+1.64
	C′ → D′	4	0	0.310 → 0.256	-0.38	1.24 → 3.00	+1.66
	A′ → E′	10 → 4	-1.71	0.295	0	1.19 → 1.93	+0.95
	F′ → D′	10 → 4	-1.71	0.256	0	2.54 → 3.00	+0.33
	A′ → D′	10 → 4	-1.71	0.295 → 0.256	-0.28	1.19 → 3.00	+1.73
	B′ → C′	10 → 4	-1.71	0.245 → 0.310	+0.47	2.85 → 1.24	-1.57
	A′ → C′	10 → 4	-1.71	0.295 → 0.310	+0.10	1.19 → 1.24	+0.08

The material parameters to meet the above condition can be obtained by solving Eq (8) for the point of bubble collapse. The results are

$$\frac{\ell}{h} = \frac{\left(\frac{ab}{2} + \frac{3}{4}\right) - \sqrt{\frac{3ab}{2}}}{\left(\frac{ab}{2} - \frac{3}{4}\right)^2} \tag{10}$$

$$\frac{d_o}{h} = \frac{4}{3ab}\left(\frac{h}{\ell}\right) - \left(\frac{2}{3} + \frac{1}{ab}\right) \tag{11}$$

where d_o is the collapse diameter of the self-biased bubble. Equation (11) is plotted as a function of $1/q$ in Figure 6 along with h/ℓ which is the reciprocal of Eq (10). As can be seen from Figure 6, the diameters (tuned to free bubble collapse) do not vary appreciably for reasonable variations of q. For example, they increase less than 20 percent over $2 \leq q \leq \infty$.

The temperature coefficients of ℓ and q to satisfy the above condition (10) can be obtained by differentiating it with respect to T. The result can be written in the form

$$\ell_T = C_b\, q_T \tag{12}$$

where

$$\ell_T = \frac{1}{\ell}\frac{\partial \ell}{\partial T}$$

$$q_T = \frac{1}{q}\frac{\partial q}{\partial T}$$

and

$$C_b = \frac{\left[-ab^2 + 3b\sqrt{\frac{3ab}{2}} - \frac{9}{2}b + \frac{3}{2}\sqrt{\frac{3b}{2a}}\right]\left(\frac{1}{q}\right)}{2a\left(ab - \frac{3}{2}\right)\left(ab + \frac{3}{2} - 2\sqrt{\frac{3ab}{2}}\right)} \tag{13}$$

The coefficient C_b is plotted in Figure 7 as a function of $1/q$. Of course, q is related to ℓ through Eq (10), which we have plotted in Figure 6. It is seen from Figure 7 that ℓ_T and q_T must have opposite signs and that $|\ell_T|$ must be less than two tenths of $|q_T|$ for $q > 2$.

Thus, we have established a more rigorous physical basis upon which self-biased films can be prepared.

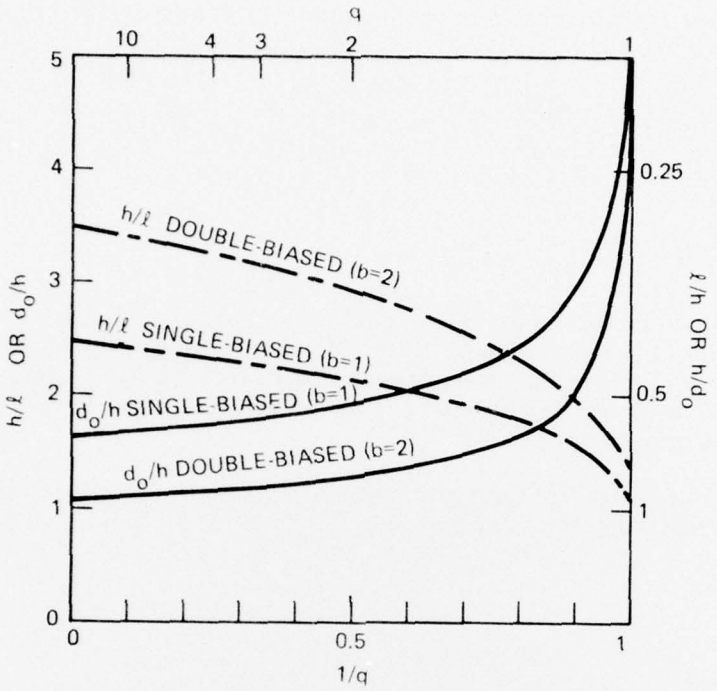

Figure 6. Variation of d_o and ℓ with q

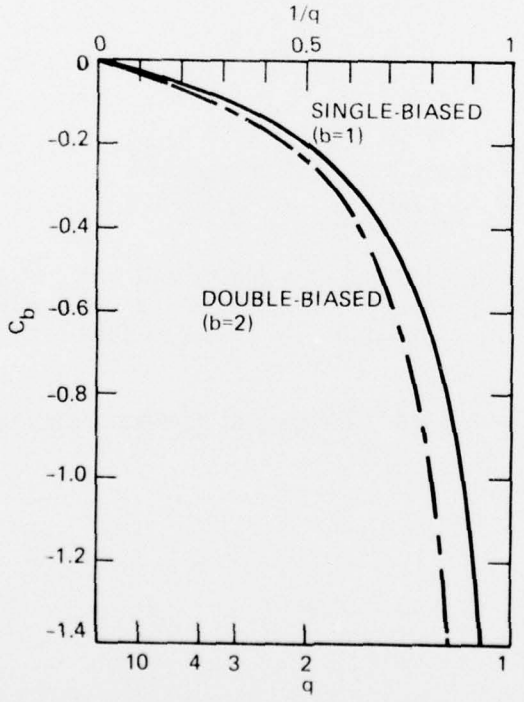

Figure 7. Dependence of C_b on q

SECTION IV

SELF-BIASED MATERIALS AND DEVICES

In the preceeding section we have derived a more rigorous expression for the effective bias field of the self-biased structure. On the basis of this we have discussed conditions for temperature-stable self-biasing. During the next six months we will grow self-biased films according to the specifications we have derived and examine their validity. In the meantime, however, several film samples designed to support self-biased bubbles of ~4 μm diameter have been grown on a company IR&D program. It was decided that an evaluation of these films using conventional 16 μm period device structures would be carried out on this program to provide baseline data from which to devise small bubble self-biased compositions and to design improved propagation structures.

Previous studies in Japan (Ref 6), which were confirmed in our laboratory, showed that it is necessary to isolate areas of the self-biased film in such a fashion that there is no residual damage to the edges of the biasing layer. Unless this is done one cannot achieve a stable saturated (single domain) state in the bias layer. Several processing methods were considered and candidate approaches were selected for evaluation.

An experiment was conducted to determine if the required isolation of islands (device areas) of the magnetic garnet film could be achieved solely by chemical etching rather than by mechanical sawing followed by a damage removal etch. A wafer with a single film of normal bubble domain material was coated with ~1 μm of sputtered SiO_2. A grid pattern of "streets and avenues" was then opened in the SiO_2 layer by conventional photolithographic techniques. This left a pattern of SiO_2 islands on top of the garnet film. The wafer was then etched in hot phosphoric acid using the SiO_2 as an etch mask. Many of the garnet film islands formed by this technique can be placed in a saturated (single domain) state so that this approach should indeed be suitable for use with the double layer self-biased films. An example of the garnet film island formation described above is shown in Figure 8. In this photograph it can be seen that one of the islands is in a saturated (single domain) state and the other one is in a demagnetized (multidomain) state. The double and triple layer film samples in which we hoped to obtain self biased bubbles of 4 μm diameter for device evaluation have been etched in the same fashion.

Difficulties in characterization of self-biased films have arisen and the sources of problems analyzed. The procedures used for single layer films rely on measurement of film thickness (h), zero field stripwidth (w), collapse field (H_o) and Neel Temperature (T_N). For the samples shown later in Table 3, the bubble material film thickness is only about 2 to 3 times the biasing layer thickness. Hence, normal optical spectrophotometer measurements cannot be used to extract the separate layer thicknesses. Measurement of bubble collapse presents no real problems, except that the theory must be modified to include the effective field from the biasing layers. Measurement of zero field stripwidth will not yield the usual information because of the biasing layers. Finally, one can readily measure T_N for self biased layers, but in the case of such films, h, w, H_o, and T_N will not yield q as it does for single layer films.

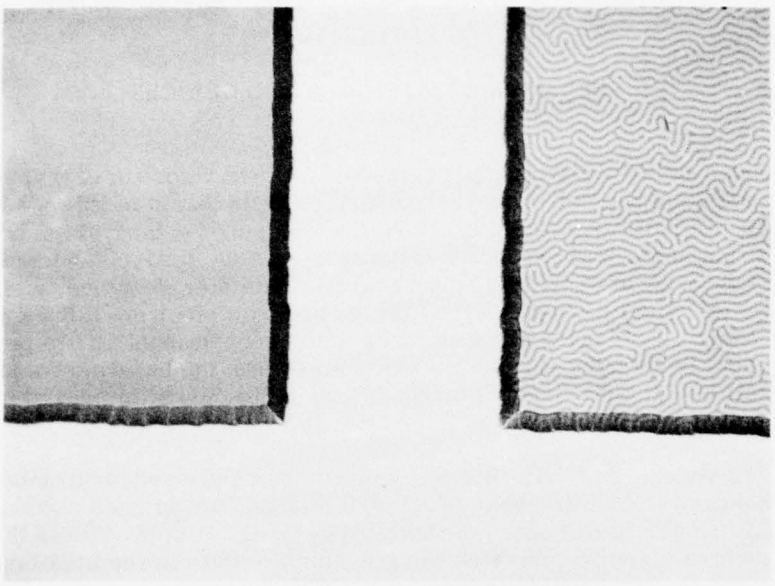

Figure 8. Islands of Garnet Film Isolated by Chemical Etching

One can see both how the problem arises and the solution to the problem by the following theoretical considerations. Suppose we have measured h by progressively measuring the film thickness as the composite structure is grown. Now for single layer films, one would next measure w which leads, with the known value of h, to the value of ℓ. This can be done because the total energy per unit area for an array of stripe domains is given by

$$E_T = E_W + E_H + E_D \tag{14}$$

where E_W is the wall energy, E_H is the Zeeman energy and E_D is the demagnetizing energy.

Minimizing E_T for a single layer film leads to the analytic result relating ℓ, w and h. The problem in the case of the biasing layer arises from the need to include another wall energy term. The net effect is to add a term to the total energy which is an effective field ($ab\sigma_W/2hM_S$) where a and b have been defined in the previous section. We can use the Kooy and Enz (Ref 11) results by simply replacing H_B in their equations by $\left(H_B - \frac{ab\sigma_W}{2hM_S}\right)$. The net result is that if we apply a field $H_{eff} = \frac{ab\sigma_W}{2hM_S}$ which cancels the biasing effect, we can use the Fowlis and Copeland results (Ref 12) to calculate ℓ from w and h. The collapse field (H_O), ℓ, h and M_S are related by

TABLE 3
Characterization Data on Multilayer Films

Sample No. D-28	Temp	0°C	25°C	50°C
	h (μm)	1.14	1.14	1.14
	w (μm)	6.15	4.50	4.65
	H_0^+ (Oe)	87.5	83	75
	ℓ (μm)	0.64	0.53	0.54
	$4\pi M_s$(G)	233	219	198
	σ_w (erg/cm^2)	0.28	0.20	0.17
	ℓ/2h	0.27	0.22	0.23
	$H_{eff}/4\pi M_s$	0.27	0.21	0.21
Sample No. D-27	**Temp**	**0°C**	**25°C**	**50°C**
	h (μm)	1.20	1.20	1.20
	w (μm)	5.06	4.00	3.33
	H_0^+ (Oe)	75	70	65
	ℓ (μm)	0.58	0.49	0.43
	$4\pi M_s$(G)	200	184	167
	σ_w (erg/cm^2)	0.18	0.13	0.10
	ℓ/2h	0.25	0.21	0.19
	$H_{eff}/4\pi M_s$	0.22	0.20	0.17
Sample No. T-26	**Temp**	**0°C**	**25°C**	**50°C**
	h (μm)	0.9	0.9	0.9
	w (μm)	3.41	3.15	3.0
	H_0^+ (Oe)	105	105	100
	ℓ (μm)	0.41	0.38	0.37
	$4\pi M_s$ (G)	182	185	177
	σ_w (erg/cm^2)	0.11	0.10	0.09
	ℓ/2h	0.23	0.21	0.21
	$H_{eff}/4\pi M_s$	0.26	0.26	0.24

$$\frac{H_o^{\pm}}{4\pi M_s} = 1 + \frac{3}{4}\frac{\ell}{h} - \sqrt{3\frac{\ell}{h} \pm \frac{H_{eff}}{4\pi M_s}} \quad ; \quad \frac{H_{eff}}{4\pi M_s} = \frac{b\ell}{2h}\left(1 - \frac{1}{q}\right)^{1/2} \tag{15}$$

Where the upper sign corresponds to the case in which the capping wall is formed outside the bubble, thus the effective bias field is subtractive from the external bias.

The explicit appearance of q in this expression and the previous one prohibits us from calculating $4\pi M_s$ for finite q values. The only alternative is to assign a value to q or to make an additional measurement involving only ℓ, h, $4\pi M_s$ and q.

The additional measurement is obviously satisfied by a measurement of the field applied to give M=O for the bubble film. Since M=O corresponds to a maximum intensity for the first order diffraction from a stripe domain film, it seems natural to use the spatial filtering characterization (SFC) technique (Ref 2) to optoelectronically extract H_{eff}. To obtain variable temperature data, it will be necessary to construct a SFC apparatus with low and high temperature capabilities. We are presently evaluating plans for the implementation of this project. From the characterization point of view, there are several advantages to such a tool. One can easily extract w, H_{eff}, and M_s from the position and field dependences of the 1st and 2nd order diffracted waves with quite high precision and eliminate measurement of H_o.

The only quick cure for obtaining characterization data is to assign q a value and extract M_s. We have tentatively chosen q=5 (this seems more realistic than q=∞) and analyzed the data at 0, 25 and 50°C for three multilayer self-biased samples, D-27, D-28, and T26. D-27 and D-28 are double layer films with a biasing layer at the bottom. T-26 is a triple layer film with a biasing layer at the bottom and a planar-magnetic layer on top. Also given in Table 3 are $\ell/2h$ and $H_{eff}/4\pi M_s$. H_{eff} was measured by applying a bias field so as to make equal the widths of the strip domains magnetized in the opposite directions (M=O). This measurement is not as accurate as the M=O measurement by the SFC technique. Nevertheless, the fact that $H_{eff}/4\pi M_s$ is slightly smaller than $\ell/2h$ for the two double layer films seems to support our theory that $H_{eff}/4\pi M_s$ is the product of ℓ/h and $(1 - 1/q)^{1/2}$. T-26 seemingly contradicts our theory. But this discrepancy may be attributed to a possible bias effect from the planar-magnetic layer and/or incorrect material parameter values which were obtained without taking account of the effect of the planar-magnetic layer.

Processing steps have begun to fabricate 20K bit devices on the above three samples.

SECTION V

HIGH DENSITY CHIP DESIGN

The basic hybrid chip organization has been described in a recent paper (Ref 13) and the composite chip concept is summarized in a second paper. (Ref 14).

To reduce these concepts to practice, there are several design aspects to be evaluated first. These include the interface element, I/O expansion circuit, decoder and transfer switches, and on-chip correction scheme. These are separately described in the following:

5.1 INTERFACE ELEMENT DESIGN

The key element for the large capacity chip through mask composition relies on the interface element between adjacent patterns. The amount of tolerable geometry distortion in these patterns determines the minimum circuit period that can be allowed under certain mask composition accuracy. The effect of geometry distortion will be studied by test circuits with controlled distortion. An example is shown in Figure 9. It consists of a number of straight propagation paths. Each path is 20 periods long and connected to the adjacent path through interface elements. By controlling the relative placement of these paths the geometry distortion due to mask composition misalignment can be simulated and thus can be evaluated through propagation margin measurement.

The circuit shown in Figure 9 consists of 16 μm period C elements. The simulated misalignment is ±2 μm in both X and Y axis. Visual observation of propagation on these circuits shows that bubbles can tolerate this type of geometry distortion with little margin degradation. A quantitative measurement will be made later.

Several new test patterns are being designed including the asymmetric half disk circuit design. The circuit will be in a closed loop form instead of a straight line so that the propagation margin data can be taken more accurately than that for a straight path.

5.2 I/O EXPANSION CIRCUIT

As the circuit period is scaled down it was found that the control currents approximately remain the same. Thus for small bubble circuits the current density in the control elements becomes the major limiting factor. To ease this restriction, it is proposed to expand the circuit period in the I/O section.

It was observed in the replicating type generator that the seed bubble can travel around the periphery of a disk or square element at much higher speeds than through a T-bar type propagation circuit. Thus, it is possible to propagate bubbles on circuits with periods much greater than the nominal criterion of four times of the bubble diameter provided the potential well under the circuit travels smoothly with the inplane rotating field as in the case of the circular disk or an equivalent pattern. This criterion can be met with the present C circuit or half disk circuit design where bubbles are essentially propagating along a smooth permalloy boundary. A test circuit is being designed to evaluate this concept.

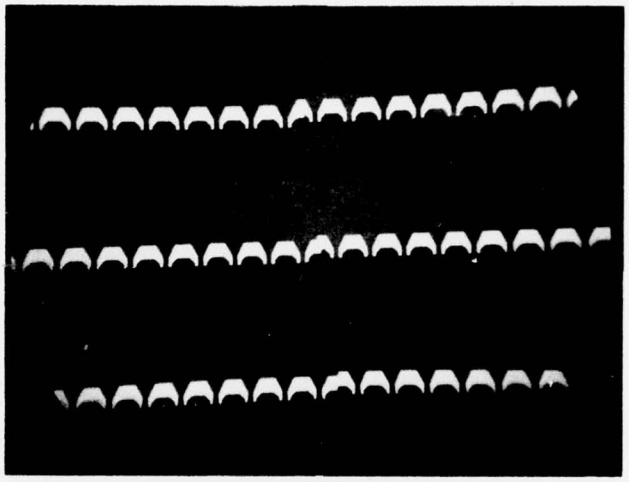

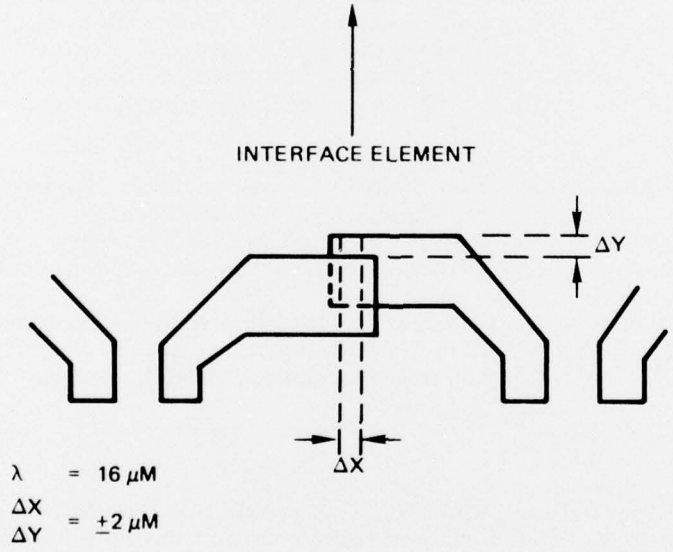

Figure 9. A Test Circuit for Studying the Interface Element

5.3 DECODER AND TRANSFER SWITCH DESIGNS

A series of retarding type decoder switches are being designed. The design goal is to establish a low power retarding switch which may operate with the same operating margin as the propagation circuit. The basic design uses a straight conductor line crossover of the propagation element. When a current pulse is passing through the conductor, it may generate either an attractive pulse or a repulsive pulse which will hold the bubble from propagating forward, thus retarding the propagation by one cycle. The propagation element used is the same as in the normal path and the variation parameter is the conductor width and placement.

Besides the retarding switch, the possibility of using a transfer switch between two parallel paths as a decoder switch will also be explored. This type of switch is intrinsically more difficult to design than the retarding type switch. It does not however require a time slot for the retarded bubble, thus it requires less space and less decoding delay than the retarding type decoder.

5.4 ON-CHIP CORRECTION SCHEMES

To achieve a reasonable yield for the large capacity chip it is essential to have fault tolerant capability in the storage organization. Because of the large block capacity in the present design it is unlikely that it will be possible to adopt the same off-chip correction approach proposed in multiple storage loop major-minor type organization. Therefore, different on-chip correction schemes have to be developed. The simplest approach involves a physical correction on the permalloy propagation path. The basic concept is as follows: a chevron propagation path is expanded vertically and splits into two different paths. By selectively etching one of the paths away the bubble is forced to propagate through the remaining path. The reason for using a multiple chevron design is its tolerance to minor geometry imperfections. Thus, a certain misalignment is allowed during the selective etching process. The other advantage of using this type of structure is that it can be used as a bias controllable passive replicator. At low bias field, the bubbles are fully stretched in this circuit and can be replicated into two for each propagation path. However, when the bias field is high, bubbles will not be fully stretched and will shrink to the top edge of the chevron track and only propagate along one path. Therefore, there are two propagation states, replicate and non-replicate, in this circuit arrangement, and they can be controlled through bias pulsing. This propagation characteristic can be used for wafer level testing in selecting the defect free propagation paths.

SECTION VI

SYSTEM CONCEPTS STUDY

As of this time only certain preliminary and general system considerations have been evaluated. Some system aspects such as the chip to electronics interface are of immediate interest because the chip design and organization is constrained by the number of components, the power, etc. of the system. Therefore, most of the systems analysis support for this program will be directed towards projecting conceptual chip organization and parameters to a 10^{12} memory by analytical and graphical methods.

Tradeoff studies have been started to determine the optimum chip organizations that would result in the best system design with respect to number of components, modular arrangements and physical construction. System parameters to be studied are:

1. Chip organizations
2. System module size
3. Multiple signal bus arrangements
4. Fault tolerant loop selection
5. Controller requirements
6. System data rates
7. System power
8. System physical size, weight, etc.

The basic system model is shown in Figure 10 and consists of a controller and a number of memory module units. Each module unit must be self-contained and be operated using a signal and control bus system. A graph was made showing the number of chips and modules required for a 10^{12} system using chips with a 1.6×10^{8} bit capacity.

In order to obtain the system data rate of 50 MHz a number of chips in parallel must be processed. Figure 11 shows this number as a function of the basic field rotational rate and the number of detector outputs from a chip.

The full results of the system conceptual study will be presented in the next interim report. (see also Ref 15)

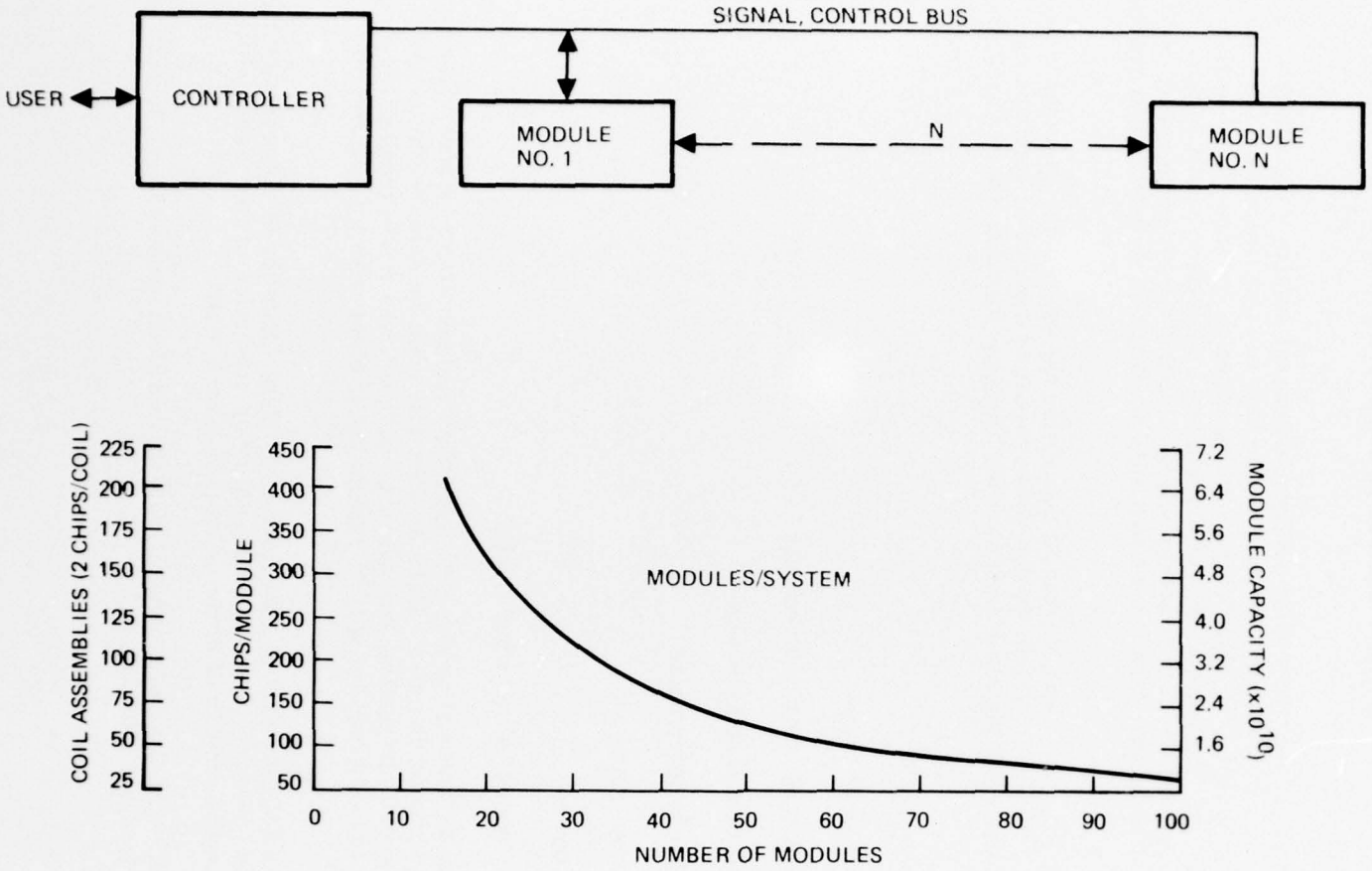

Figure 10. 10^{12} Bit System Model

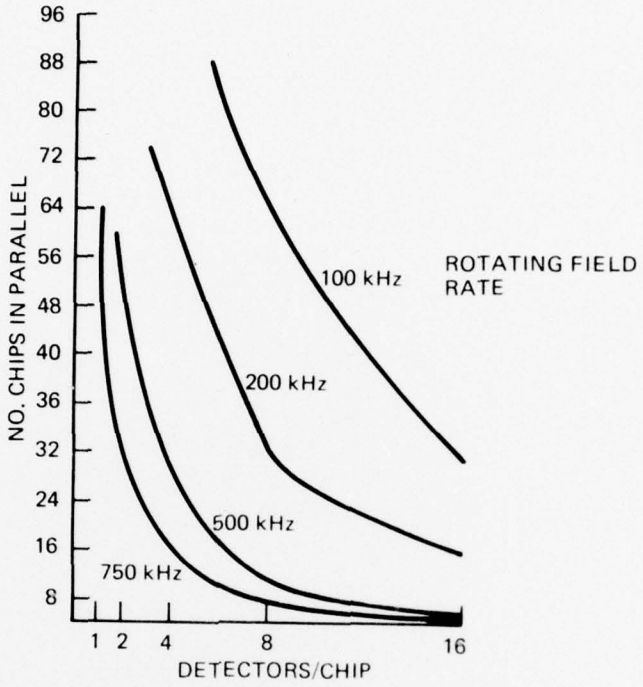

Figure 11. Design Considerations for 50 MHz Data Rate

SECTION VII

SUMMARY

Encouraging small bubble material properties have been obtained with an YSmTmGaIG composition. Film samples have been submitted for device evaluation at both 8 μm and 4 μm periods. A Ge-substituted variation of this composition is being formulated to extend the temperature range of operation.

A more rigorous analysis of self-biased structures has been carried out. The results provide better insight into the criteria that the material parameters and device structures must satisfy for stable variable temperature operation. Preliminary material and device processing studies have been initiated on self-biased structures. The design of components to test the hybrid chip and wafer level integration concepts is proceeding. A test chip has been submitted to CAD (computer aided design).

The system concepts study is at an early stage but will be completed in the interval of the next interim report.

In general the program is proceeding on schedule and according to plan.

REFERENCES

1. R. W. Shaw, D. E. Hill, R. M. Sandfort and J. W. Moody, "Determination of Magnetic Bubble Film Parameters from Strip Domain Measurement," J. Appl. Phys. 44, 2346 (1973).

2. R. D. Henry, "Bubble Material Characterization Using Spatial Filtering," Mat. Res. Bul. 11, 1285 (1976).

3. T. W. Liu, A. H. Bobeck, E. A. Nesbitt, R. C. Sherwood, and D. D. Bacon, "Thin-Film Surface Bias on Magnetic Bubble Materials," J. Appl. Phys. 42, 1360 (1971).

4. A. H. Bobeck, S. L. Blank, and H. J. Levinstein, "Multilayer Epitaxial Garnet Films for Magnetic Bubble Devices - Hard Bubble Suppression," Bell Syst. Tech. J. 51, 1436 (1972).

5. H. Uchishiba, H. Tominaga, T. Namikata, and S. Sakai, "Internal Bias Effect of Double Layer Epitaxial Garnet Films," IEEE Trans. Magn. MAG-9, 381 (1973).

6. H. Uchishiba, H. Tominaga, T. Obakata, and T. Namikata, "Growth and Properties of Stable Self Biasing Double Layer Epitaxial Garnet Films," IEEE Trans. Magn. MAG-10, 480 (1974).

7. H. Uchishiba, H. Tominaga, and K. Asama, "Temperature Stable Self-Biasing Bubbles in Double Layer Films," IEEE Trans. Magn. MAG-11, 1079 (1975).

8. A. A. Thiele, "The Theory of Cylindrical Magnetic Domains," Bell Syst. Tech. J. 48, 3287 (1969).

9. W. J. DeBonte, "Stability of Half-Bubbles in Double-Layer Films," AIP Conf. Proc. 10, 349 (1972).

10. H. Callen and R. M. Josephs, "Dynamics of Magnetic Bubble Domains with an Application of Wall Mobilities," J. Appl. Phys. 42, 1977 (1971).

11. C. Kooy and U. Enz, "Experimental and Theoretical Study of the Domain Configuration in Thin Layers of $BaFe_{12}O_{19}$," Philips Res. Repts. 15, 7 (1960).

12. D. C. Fowlis and J. A. Copeland, "Rapid Method for Determining the Magnetization and Intrinsic Length of Magnetic Bubble Domain Materials," AIP Conf. Proc. 5, 240 (1971).

13. T. T. Chen, I. S. Gergis and T. R. Oeffinger, "A Hybrid Decoder Bubble Memory Organization" IEEE Trans. Magn. MAG-12, 630, (1976).

14. T. T. Chen and J. P. Peekstin "Large Capacity Bubble Memory Chip through Wafer Level Integration," Presented at the International Conference on Magnetic Bubbles, Eindhoven, Sept, 1976.

15. T. T. Chen and B. A. Waggoner, "10^{12} Bit Bubble Memory System" to be presented at the National Aerospace and Electronics Convention (NAECON), Dayton, Ohio, May 17-19, 1977.

☆ U. S. GOVERNMENT PRINTING OFFICE: 1977 — 757-001/539